Even-odd interference effect in a topological superconducting wire

Jie Liu,[1] Juntao Song,[2] Qing-Feng Sun,[3,4] and X. C. Xie[3,4]

[1]*Department of Applied Physics, School of Science, Xian Jiaotong University, Xian 710049, China*

[2]*Department of Physics and Hebei Advanced Thin Film Laboratory, Hebei Normal University, Shijiazhuang 050024, China*

[3]*International Center for Quantum Materials, School of Physics, Peking University, Beijing 100871, China*

[4]*Collaborative Innovation Center of Quantum Matter, Beijing 100871, China*

(Received 19 May 2017; revised manuscript received 21 August 2017; published 27 November 2017)

We study the nonlocal transport property of Majorana quasiparticle states (MQPs) in a normal lead–topological superconducting wire–normal lead system. We find that the tunneling coefficient of the electron transmission process displays an interesting even-odd interference behavior. However, this even-odd interference behavior is difficult to observe in the tunneling coefficient of the crossed Andreev reflection process (CAR). We show that this even-odd interference behavior is directly related to the self-Hermitian property of MQPs. Due to the self-Hermitian property, the correction to the transport in the electron transmission process is in the first order while the correction to the CAR process is in the higher order. Thus, the interference behavior is more significant in the electron transmission process than in the CAR process. Such a unique transport property demonstrates the nonlocal and self-Hermitian characteristics of MQPs.

DOI: 10.1103/PhysRevB.96.195307

I. INTRODUCTION

Due to the unique non-Abelian braiding statistical property of Majorana quasiparticle states (MQPs), they can form the building blocks of a topological quantum computer [1–3]. Thus, realizing MQPs in a laboratory setting has become a major focus in condensed-matter physics. Kitaev suggested that MQPs can appear as quasiparticle end states in a one-dimensional (1D) p-wave superconductor [4]. However, because 1D p-wave superconductors are rare in nature, various experimentally feasible proposals based on a hybrid of a conventional superconductor and a low-dimensional system have been put forward [5–14]. Among these proposals, a semiconductor wire exposed to an external magnetic field and with proximity-induced superconductivity has been singled out as the most feasible device. Through the advancements in nanotechnology, an experimental work towards this goal was shown by Kouwenhoven's group [15]. They successfully fabricated a topological superconducting system based on the semiconductor wire and observed the signal of zero bias peak as indicated by the theory [16,17]. Following Kouwenhoven's work, many groups successfully fabricated semiconductor-superconducting wires and observed a similar phenomenon [18–21]. In addition to the semiconductor systems, a topological superconducting system consisting of ferromagnetic atomic chains placed on a trivial superconductor has been experimentally realized [22]. Although the results of these experiments—in particular whether MQPs have really been detected—have been hotly debated [23–27], significant advancements in fabricating high-quality hybrid nanowire-superconductor samples have been achieved lately, and the renewed experiments demonstrate the plausibility of MQPs [28–31]. For example, Kouwenhoven *et al.* constructed a ballistic semiconductor superconducting wire and detected a clear zero-bias peak [28]. Such a highly clean system can eliminate the effect of disorder, making the results more plausible. At the same time, great progress has also been made in atomic chain topological superconducting systems, where Yazdani's group recently provided a high-resolution MQP signal [32]. The more exciting achievement is the topological insulator-superconductor hybrid system, which is another theoretically proposed hybrid topological superconducting system [5]. Several groups have successfully fabricated superconductor-topological insulator-superconductor systems and observed unusual Josephson effects in such a system [33–38]. These improved results certainly demonstrate the presence of MQPs.

Although huge advances have been achieved in experiments, an admitted method for definitely distinguishing MQPs in experiment is still an open question. Recent strategies can be classified into two camps. One strategy is to combine more topological superconducting wire together to realize more exotic MQP properties. In such complex systems, the fractional Josephson effect is another landmark of topological superconductor. Quite recently, some fractional Josephson effect signals [36–38] were observed in a topological insulator system. However, the fractional Josephson effect has still not been well observed in a semiconductor superconducting wire system, although Kouwenhoven's group and Marcus' group successfully fabricated semiconductor superconducting Josephson junctions [39–41]. In principle, the fractional Josephson effect can be easily spoiled by quasiparticle poisoning, as shown in a series of theoretical works [42–49]. Another strategy is to uncover more unique properties of MQPs in a single wire system. For example, by definition, a MQP's wave function must be self-Hermitian; such a property results in the well-known equal-spin Andreev reflection [50], which was recently verified by Jia's group [51]. Another unique MQP property is that MQPs must be nonlocally distributed at both ends of the wire. Two MQPs can combine to form a nonlocal state. Thus, two different nonlocal transport processes can arise. One such process is the crossed Andreev reflection (CAR), where two electrons from different ends can combine to form a Cooper pair with the aid of two MQPs [52–55]. The second process is electron teleportation, where a single electron can be teleported from one end to the other end with the aid of two MQPs in the Coulomb blockade regime [56]. Recently, the electron teleportation process has been demonstrated by

Marcus' group and used directly to demonstrate the existence of MQPs [29]. However, further research by Marcus' group showed that quasiparticle poisoning can also lead to similar electron teleportation phenomena [31]. Thus, uncovering more unusual nonlocal transport properties of MQPs is essential for further distinguishing MQPs.

Furthermore, two nonlocally distributed MQPs can constitute the basis of a topological qubit. They combine to form a nonlocal fermion state, which can be either empty or occupied. These two states are characterized by an even or odd fermion parity state. For a finite-sized wire, two MQPs at the two ends of the wire can interact with each other through the wire. This causes the energy spectra of the even and odd parity states to oscillate with varying parameters, such as chemical potential and Zeeman field. Because of this oscillatory behavior, the two states cross each other at the zero point and thus switch the fermion parity of the ground state correspondingly. This parity switching behavior is quite useful. As shown in Ref. [57], the ability to tune the parity of MQPs may provide a powerful way to perform certain non-Abelian rotational operations. Thus, revealing the parity of MQPs through transport properties can further benefit quantum computing. Although the density of states can distinguish the difference, it does not provide a concrete transport-based method to reveal the parity of MQPs, following the literature report [58]. Furthermore, recent researches suggest that electron teleportation can be used for non-Abelian braiding of MQPs [59,60], a significant milestone towards topological quantum computing. Thus, combining the parity information and electron teleportation properties of MQPs can certainly result in more meaningful applications for future quantum computing and would be beneficial to further uncover the exotic nonlocal transport properties of MQPs in finite-sized wire.

In this study, we focused on the nonlocal transport properties of MQPs in a normal lead–topological superconducting wire–normal lead (NSN) system. Such an NSN system has been extensively studied [52–54,61]. However, most previous researches focused on the properties of the CAR process or the nonlocal correlation between the two leads. Very limited research has been carried out on the electron transmission (ET) process where an electron can be transmitted from one side to the other side with the aid of MQPs. Figure 1(a) shows an experimental setup revealing both the ET and CAR processes. We find that the nonlocal transport can be further modified by the finite-size effect. In addition, the correction to the ET process can directly manifest the information of even-odd parity. The resonant peak value of the ET tunneling coefficient is proportional to $1+(-1)^{N_v} b \sin(k_F L)$ with $N_v = 0/1$, corresponding to the even/odd parity state (here k_F is the Fermi wave vector, L is the length of the topological superconducting wire, and b is a small constant determined by the finite-size effect). However, such parity-related interference behavior is hard to observe in the CAR process. We further investigated the underlying mechanisms that drive the different transport behaviors for the two nonlocal processes, and found that different transport behaviors are directly related to the self-Hermitian property of MQPs. Because of this self-Hermitian property, the correction to the ET process is a first-order correction, while the correction to the CAR process is a higher-order one. Thus, the even-odd

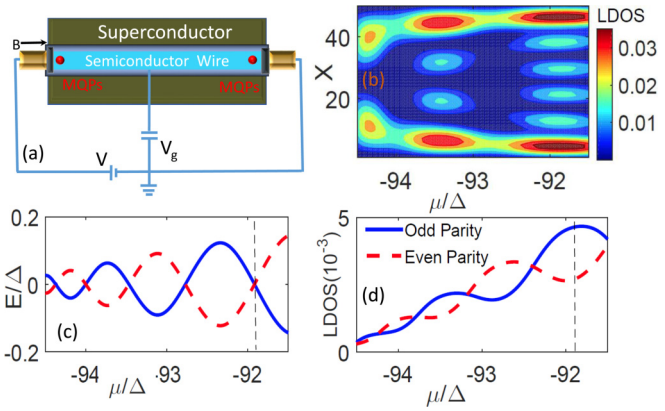

FIG. 1. (a) A schematic setup with two normal-metal leads coupled to a superconducting wire to form an NSN system. (b) Electron local density of states (LDOS) for odd parity states vs the chemical potential and position. The MQPs are mainly localized at the two ends of the wire. Another feature of MQPs is that the electron LDOS of MQPs oscillates with the chemical potential. (c) The energy spectra of two hybridized states of MQPs. They are even-odd parity correlated and oscillate with the chemical potential. (d) The electron LDOS of the two hybridized states also displays the even-odd parity correlated interference pattern. Here red dashed line (blue solid line) means even (odd) parity state. The LDOS locates at the position $X = 1$. The parameters are $N_x = 100a$, $N_y = 5a$, $U_R = 2\Delta$, $V_x = 2\Delta$.

interference behavior is more significant in the ET process. Such a unique transport property reveals the nonlocal and self-Hermitian properties of MQPs.

The rest of this study is organized as follows: In Sec. II, the Hamiltonian of a semiconductor superconducting wire is introduced, and the formula for the nonlocal current is presented. In Sec. III, the numerical and analytical results are divided into four parts. In Sec. III A, we show numerically that the local density of states is correlated to the parity and further affects the nonlocal transport properties of the MQPs. In Sec. III B, the analytical results and reasons for the unique nonlocal transport properties of the MQPs are provided. In Secs. III C and III D, the effect of Zeeman field and disorder is shown. Finally, a brief summary is given in Sec. IV.

II. HAMILTONIAN OF SEMICONDUCTOR SUPERCONDUCTING WIRE AND CURRENT FORMULA

Figure 1(a) shows the setup of an NSN system. The topological superconducting wire used is a quasi-1D s-wave superconductor with the Rashba spin-orbit coupling. The tight-binding model based on Refs. [12,23] is as follows:

$$\begin{aligned} H_{q1D} = & \sum_{\mathbf{R},\mathbf{d},\alpha} -t(\psi^\dagger_{\mathbf{R}+\mathbf{d},\alpha}\psi_{\mathbf{R},\alpha} + \text{h.c.}) - \mu\psi^\dagger_{\mathbf{R},\alpha}\psi_{\mathbf{R},\alpha} \\ & + \sum_{\mathbf{R},\mathbf{d},\alpha,\beta} -iU_R\psi^\dagger_{\mathbf{R}+\mathbf{d},\alpha}\hat{z}\cdot(\vec{\sigma}\times\mathbf{d})_{\alpha\beta}\psi_{\mathbf{R},\beta} \\ & + \sum_{\mathbf{R},\alpha,\beta} \psi^\dagger_{\mathbf{R},\alpha}[(V_x\sigma_x)_{\alpha\beta} + V_{\text{imp}}(\mathbf{R})\delta_{\alpha\beta}]\psi_{\mathbf{R},\beta} \\ & + \sum_{\mathbf{R},\alpha} \Delta\psi^\dagger_{\mathbf{R},\alpha}\psi^\dagger_{\mathbf{R},-\alpha} + \text{H.c.} \end{aligned} \tag{1}$$

Here, $\mathbf{R}$ denotes the lattice sites, $\mathbf{d}$ denotes the two unit vectors $\mathbf{d_x}$,$\mathbf{d_y}$ which connect the nearest-neighbor sites in the x and y directions respectively. α,β are the spin indexes, t is the hopping amplitude, μ is the chemical potential, U_R is the Rashba coupling strength, and V_x is the Zeeman energy caused by a magnetic field along the wire in the x direction. Δ is the superconducting pairing amplitude and $V_{\rm imp}(\mathbf{R})$ is the on-site random impurity.

To analyze the nonlocal transport property of MQPs, the recursive Green's-function method is used to calculate the scattering matrix of the system. The recursive Green's-function method is a powerful method to study the transport properties of the topological superconducting system [52,62]. The scattering matrix is related to the Green's functions by

$$S_{lk}^{\alpha\beta} = -\delta_{l,k}\delta_{\alpha,\beta} + i[\Gamma_l^{\alpha}]^{1/2} * G^r * [\Gamma_k^{\beta}]^{1/2}, \qquad (2)$$

where $S_{lk}^{\alpha,\beta}$ is an element of the scattering matrix that denotes the scattering amplitude of the β particle from the kth lead to the α particle in the lth lead. l,$k = L$ or R. L and R denote the left and the right lead, respectively. α,$\beta \in \{e,h\}$ denotes the electron (e) or hole (h) channels. $G^r = [E - H_{q1D} - \sum_{l,\alpha}(\Sigma_l^{\alpha})^r]^{-1}$ is the retarded Green's function of the superconducting wire. $\Gamma_l^{\alpha} = i[(\Sigma_l^{\alpha})^r - (\Sigma_l^{\alpha})^a]$ is the linewidth function of α particle in the lth lead, where $(\Sigma_l^{\alpha})^{r(a)}$ is the α particle retarded (advanced) self-energy for the lth lead. The physical meaning of the scattering matrix is obvious: $S_{ll}^{e,h}$ means the Andreev reflection coefficient T_A in the lth lead, $S_{lk}^{e,h}$ means the CAR coefficient $T_{\rm CAR}$ from the lth lead to the kth lead, and $S_{lk}^{e,e}$ means the electron transmission coefficient T_e from the lth lead to the kth lead. For the setup shown in Fig. 1(a), the bias V is applied at the left lead while the superconducting wire and the right lead are grounded. Thus, the relationships between the current and tunneling coefficient are $I_L = \frac{e}{h}\int dE[T_A(f_{Le} - f_{Lh}) + (T_e + T_{\rm CAR})(f_{Le} - f_R)]$ and $I_R = \frac{e}{h}\int dE(T_e - T_{\rm CAR})(f_{Le} - f_R)$. Here, $f_{Le/h} = f(E \mp V)$ means the Fermi distribution function of electrons/holes in the left lead and $f_R = f(E) = [1 + \exp(E/k_BT)]^{-1}$ means the Fermi distribution function in the right lead. At zero temperature, the differential conductance is given by $G_R = \frac{\partial I_R}{\partial V} = \frac{e^2}{h}(T_e - T_{\rm CAR})$. Thus, the current at the right lead is mainly determined by the nonlocal ET and CAR processes. In the following calculation, only the tunneling coefficient of ET and CAR is shown, providing clearer transport property information than the current.

III. NUMERICAL RESULTS AND DISCUSSION

With the given model and formulas, the nonlocal transport property of MQPs is calculated. According to the experiment in Ref. [15], the superconducting gap is approximately 250 μeV and the spin-orbit coupling strength is 20 meV nm. Thus, $\Delta = 250$ μeV was set as the unit energy, and the lattice constant $a = 20$ nm. Other parameters are $t = 25\Delta$, $U_R = 2\Delta$, and $V_x = 2\Delta$. The nontrivial region lies in the range $-\sqrt{V_x^2 - \Delta^2} < \mu - \mu_N < \sqrt{V_x^2 - \Delta^2}$ (where μ_N is the chemical potential at the bottom of the Nth band).The nonlocal transport properties of MQPs are present in a grounded superconducting wire when the wire length is finite, as shown in the literature [52]. Wire dimensions were chosen as $N_x a \approx 1$ μm and $N_y a \approx 100$ nm. The wire length is about twice the superconducting coherence length ξ_0 and about half the wire length used in the experiment of Ref. [15].

A. Parity correlated energy states, local density of states, and transport property in a short topological superconducting wire

In this section, we present the relation between the parity and the energy spectrum, and show how to determine the parity through the local density of states. In a short wire as shown in Fig. 1(c), the energy of the in-gap states versus the chemical potential exhibits an oscillatory behavior in the topologically nontrivial regime because of the coupling between the two MQPs. This differs from the long wire case, where energy remains close to zero. In general, the coupling energy of the two MQPs are $E_M \approx k_F \frac{e^{-L/\xi}}{\xi}\cos(k_F L)$ [63–65], where L is the length of the topological superconducting wire and $k_F \approx \sqrt{\sqrt{V_x^2 - \Delta^2} + \mu}$ is the effective Fermi wave vector which is a function of the chemical potential μ and the Zeeman field V_x. The coupling energy can be further related to parity. As is known, a single MQP has just half of the degree of a conventional fermion, and two MQPs can combine to form a conventional fermion via the relationship $\psi = (\gamma_1 + i\gamma_2)$. When the two MQPs hybridize together, the effective Hamiltonian in the conventional fermion basis can be written as $H_{\rm eff} = iE_M\gamma_1\gamma_2 = 2E_M(\hat{N} - 1/2)$, where $\hat{N} = \psi^{\dagger}\psi$ is the number operator. Then, $N_v = \langle\hat{N}\rangle = 1$ corresponds to the odd-parity state where energy $E = E_M$ and $N_v = \langle\hat{N}\rangle = 0$ corresponds to the even-parity state where energy $E = -E_M$ (the parity can be calculated through a more general method via the Pfaffian of the transformation matrices in Ref. [57]). Moreover, E_M can be adjusted through the chemical potential and the Zeeman field. Figure 1(c) shows the energy spectra of these two states as a function of chemical potential. These two states cross each other at the zero point. In this case, the parity of the ground state will change with the crossing of energy spectra at the zero point. Such a parity switching process indicates that the parity of the system can be tuned through modification of the chemical potential. As shown in the literature [59,60], the non-Abelian braiding process can be operated through a sequence of projective measurement processes. However, to get a valid braiding through projective measurement, the desired parity of MQPs should be fixed. Thus, the ability to tune the parity of MQPs could benefit the projective measurement process and further topological computation and is essential to the further study of the parity information.

The parity relationship can be further examined through the local density of states (LDOS). Reference [58] showed that the parity relationship is related to the difference between the electron LDOS and the hole LDOS, while our calculations go further and show that only the electron LDOS or hole LDOS can manifest the parity information. In general, the electron LDOS is proportional to $(-1)^{1+N_v}\sin(k_F L)$ and the hole LDOS is proportional to $(-1)^{N_v}\sin(k_F L)$. Figure 1(b) shows the contour plot of the electron LDOS of the odd parity hybridized states versus the chemical potential μ and wire position X, indicating the electron LDOS is mainly localized at the two ends of the wire, consistent with the features of MQPs.

Furthermore, the electron LDOS shows an oscillating behavior with the chemical potential μ. To better view this oscillation, the LDOS at $X = 1$ was extracted, shown as the blue solid line in Fig. 1(d). Note that it does oscillate with μ. We compare this behavior to the electron LDOS of the even parity states at $X = 1$, which is shown as the red dashed line in Fig. 1(d). Indeed the LDOSs of these two states are correlated to each other and display the parity-related information; one is destructive while the other is constructive. Furthermore, the oscillation behavior of electron LDOS is proportional to $\sin(k_F L)$ while the oscillation behavior of energy states is proportional to $\cos(k_F L)$, there being a $\pi/2$ phase shift between the energy and the electron LDOS. This phase shift can further help us to distinguish the parity of the two states. When $k_F L = \pi/2$, the energy states are degenerate, hence difficult to distinguish. However, the difference is clearly visible in the LDOS: the LDOS is in its maximum or minimum as indicated by the vertical dashed line in Fig. 1(d).

Figure 1 shows that the energy states and the LDOS of two hybridized MQPs are parity correlated. Next, we considered whether this parity-correlated information can be manifested in transport properties. In previous studies, researchers mainly focused on the AR or CAR properties of MQPs [52,53,61,66,67]. Those results are difficult to connect to parity. Recognizing that there is another ET process, an NSN model as shown in Fig. 1(a) was considered to investigate the interference information. Unlike the previous models, here the voltage is applied only on the left lead; the voltage on the right lead is set to zero. In this situation, the local Andreev reflection process cannot occur at the right lead; only the nonlocal transport process can occur. Figure 2(a) shows the total tunneling coefficient at the right lead; it displays a resonant peak when the incident energy equals the coupling energy of MQPs. The peak positions of the tunneling spectra vary exactly as the energy spectra in Fig. 1(c) do. They oscillate and cross at the zero energy point as the chemical potential varies. What is more, the peak values of the tunneling spectra around the zero point are positive along one species of the energy spectrum and negative along another species of the energy spectrum. They exhibit a very strange positive-negative exchange behavior as the chemical potential is located in the topological region. To further distinguish the strange behavior of the tunneling spectrum in the right lead, it was divided into two parts: ET and CAR. Figure 2(b) shows the contour plot of the ET tunneling coefficient T_e as a function of μ and E. The plot clearly shows the parity-related interference pattern. According to the energy spectra of the system, the resonant peak positions can be divided into two species: One species follows the trace of $\cos(k_F L)$ and the other follows the trace of $-\cos(k_F L)$. Interestingly, the peak values of the resonant peaks also reflect the relationship with parity. The peak value of the resonant peak along the spectrum of $\cos(k_F L)$ is proportional to $1 + b\sin(k_F L)$ and the peak value of the resonant peak along the spectrum of $-\cos(k_F L)$ is proportional to $1 - b\sin(k_F L)$, where b is a small quantity determined by the length of the wire. Therefore, the tunneling coefficient of the ET process can directly reveal the parity related interference information of MQPs. Figure 2(c) shows the contour plot of the CAR tunneling coefficient T_{CAR} versus μ and E. However, the peak value of CAR varies slightly with the chemical potential and shows nearly no interference information related to the parity. Thus, the total tunneling coefficient, $T_e - T_{\mathrm{CAR}}$, displays the positive-negative exchange behavior because of the different behaviors in the two nonlocal transport processes.

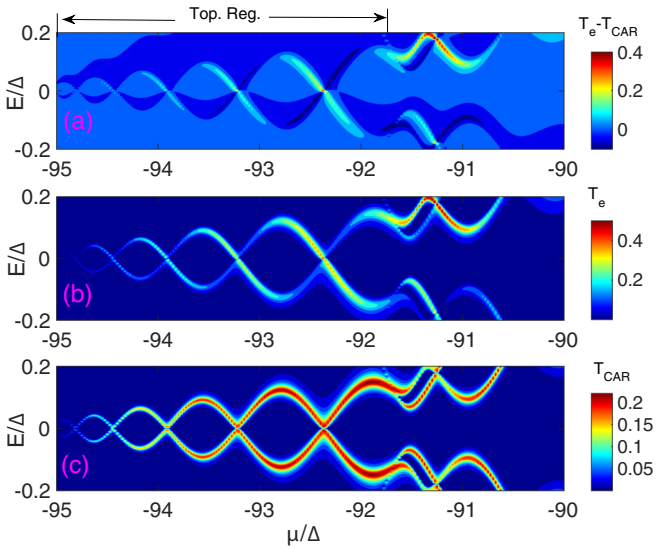

FIG. 2. The even-odd interference behavior can be detected in the right lead. (a) Contour plot of total tunneling coefficient $T_e - T_{\mathrm{CAR}}$ vs chemical potential μ and incident energy E. Here, Top. Reg. means the region for topological nontrivial region. (b) Contour plot of ET tunneling coefficient T_e vs chemical potential and incident energy E. The even-odd interference behavior can be clearly observed through ET process. (c) Contour plot of CAR tunneling coefficient T_{CAR} vs chemical potential and incident energy E. The even-odd interference behavior is nonsignificant in CAR process. The parameters are $N_x = 100a$, $N_y = 5a$, $U_R = 2\Delta$, $V_x = 2\Delta$.

B. Reason for different behaviors of CAR process and ET process

In Sec. III A we showed that the even-odd parity correlated interference information can be seen in the ET process, but is hardly visible in the CAR process. Why do these two processes exhibit distinctive behaviors? Here we try to understand the difference through the even-odd parity interference of LDOS. For a general in-gap state, the wave function can be set as $\psi = (u, \upsilon)^T$. Here, u is the electron component of the wave function and υ is the hole component of the wave function. In general, they are independent of each other, whereas for MQPs, the self-Hermitian property dictates that $u = \upsilon^*$. The two degenerate wave functions of MQPs can be given as $\psi_1 = (u_1(x), u_1(x)^*)^T$, which lies at the left end, and $\psi_2 = (iu_1(x - L), -iu_1(x - L)^*)^T$, which lies at the right end. According to Ref. [64], $u_1 = u_0 e^{ik_F x - |x|/\xi}$, where u_0 is a general form which containing spin information. Thus, the excited wave functions formed by two MQPs are represented by the following equation:

$$\psi_{\pm}(x) = \psi_1(x) + (-1)^{N_v}\psi_2(x) = \begin{pmatrix} u_1(x) + i(-1)^{N_v}u_1(x - L) \\ u_1(x) - i(-1)^{N_v}u_1(x - L) \end{pmatrix} = \begin{pmatrix} u_{\pm}(x) \\ \upsilon_{\pm}(x) \end{pmatrix}, \quad (3)$$

where, $\pm$ corresponds to $N_v = 0$ and 1, representing the even and odd parity states of the system, respectively. Thus, for a hybridized state caused by MQPs, the LDOS of electron component at the ends is $|u_{\pm,\mathrm{end}}|^2 = 1 - (-1)^{N_v} e^{-L/\xi} \sin(k_F L)$ and the LDOS of hole component at the ends is $|\upsilon_{\pm,\mathrm{end}}|^2 = 1 + (-1)^{N_v} e^{-L/\xi} \sin(k_F L)$. The LDOS oscillation is caused by the interference of two MQPs.

After the interference information of LDOS has been given, the LDOS can be related to the nonlocal transport properties of MQPs. The nonlocal transport of MQPs through scattering matrices in a topological superconducting wire system has been investigated [52,53]. However, the interference of MQPs has not been considered in these two references. To overcome this flaw, an effective Hamiltonian, $H_{\mathrm{eff}} = H_N + H_M + H_T$, is suggested as follows:

$$\begin{aligned} H_N &= -i v_f \sum_{l\in L/R} \int_{-\infty}^{+\infty} \psi_l^\dagger(x) \partial_x \psi_l(x) dx, \\ H_M &= i E_M \gamma_1 \gamma_2, \\ H_T &= \sum_l -i[\gamma_1(\tilde{t}_{l,1}\psi_{l,\mathrm{end}}^\dagger + \tilde{t}_{l,1}^* \psi_{l,\mathrm{end}}) \\ &\quad + \gamma_2(\tilde{t}_{l,2}\psi_{l,\mathrm{end}}^\dagger + \tilde{t}_{l,2}^* \psi_{l,\mathrm{end}})]. \end{aligned} \tag{4}$$

Here, H_N is the Hamiltonian of the left and right normal leads, ψ_l denotes the fermion operator of the lth normal lead, $l = L/R$ means the left/right normal lead, respectively. v_f is the corresponding Fermi velocity of the leads. H_M is the Hamiltonian of the two coupled MQPs, where E_M is the coupling strength between the two MQPs, γ_1 and γ_2. The coupling between the leads and the MQPs is described by H_T, and the coupling strengths are denoted by $\tilde{t}_{l,1}$ and $\tilde{t}_{l,2}$. In this model, H_T contains a nonlocal coupling term with a coupling strength of $\tilde{t}_{L,2}$ ($\tilde{t}_{R,1}$) between the left (right) lead and γ_2 (γ_1). The nonlocal coupling terms must go through the bulk wire to connect the leads with an exponential decay and phase shift, $k_F L$. Through the transfer wave function of MQPs, the relationship between the nonlocal coupling term and the local coupling term can be given by $\tilde{t}_{L,2} = (-1)^{N_v} e^{-L/\xi} e^{ik_F L} \tilde{t}_{L,1}$ and $\tilde{t}_{R,1} = (-1)^{N_v} e^{-L/\xi} e^{ik_F L} \tilde{t}_{R,2}$. They are parity related because the coupling term is affected by the interference of MQPs. Considering that a single MQP is just half of the ordinary fermion state, the MQP representation can be changed into fermion representation given by $\gamma_1 = d + d^\dagger$, $\gamma_2 = i(d - d^\dagger)$, As a result, H_M and H_T will change to

$$\begin{aligned} \tilde{H_M} &= E_M d^\dagger d, \\ \tilde{H_T} &= \sum_l [\tilde{t}_{l,e}\psi_l^\dagger(0) d + \tilde{t}_{l,h}\psi_l^\dagger(0) d^\dagger + \mathrm{H.c.}], \end{aligned} \tag{5}$$

with

$$\begin{aligned} \tilde{t}_{l,e} &= -i\tilde{t}_{l,1}[1 + i(-1)^{N_v} e^{-L/\xi} e^{-ik_F L}], \\ \tilde{t}_{l,h} &= -i\tilde{t}_{l,1}[1 + i(-1)^{N_v} e^{-L/\xi} e^{ik_F L}]. \end{aligned}$$

Here, $\tilde{t}_{l,e}$ exhibits the same interference pattern as $u_{\pm,\mathrm{end}}$, and $\tilde{t}_{l,h}$ exhibits the same interference pattern as $\upsilon_{\pm,\mathrm{end}}$. Thus, the effective couplings between the leads and the TS wire are renormalized by the interference of MQPs. The scattering matrix can be written in a model-independent form:

$$S(E) = 1 - 2\pi i W^\dagger (E - \tilde{H_M} + i\pi W W^\dagger)^{-1} W, \tag{6}$$

where W is the matrix that describes the coupling of the scattering to the leads:

$$W = \begin{pmatrix} \tilde{t}_{L,e} & \tilde{t}_{R,e} & \tilde{t}_{L,h} & \tilde{t}_{R,h} \\ -\tilde{t}_{L,h}^* & -\tilde{t}_{R,h}^* & -\tilde{t}_{R,e}^* & -\tilde{t}_{R,e}^* \end{pmatrix}.$$

In the weak-coupling regime, the coefficients related to the ET and CAR process can be given as

$$\begin{aligned} S_{\mathrm{LR}}^{ee} &= \frac{i\frac{\pi}{v_F}\tilde{t}_{L,e}\tilde{t}_{R,e}^*}{\left(E - E_M + i\Sigma_{l,\alpha}\frac{\pi}{v_F}|\tilde{t}_{l,\alpha}|^2\right)} \\ &\quad + \frac{i\frac{\pi}{v_F}\tilde{t}_{L,h}\tilde{t}_{R,h}^*}{\left(E + E_M + i\Sigma_{l,\alpha}\frac{\pi}{v_F}|\tilde{t}_{l,\alpha}|^2\right)}, \\ S_{\mathrm{LR}}^{eh} &= \frac{i\frac{\pi}{v_F}\tilde{t}_{L,e}\tilde{t}_{R,h}^*}{\left(E - E_M + i\Sigma_{l,\alpha}\frac{\pi}{v_F}|\tilde{t}_{l,\alpha}|^2\right)} \\ &\quad + \frac{i\frac{\pi}{v_F}\tilde{t}_{L,h}\tilde{t}_{R,e}^*}{\left(E + E_M + i\Sigma_{l,\alpha}\frac{\pi}{v_F}|\tilde{t}_{l,\alpha}|^2\right)}. \end{aligned} \tag{7}$$

When $E_M \gg \Sigma_{l,\alpha}\frac{\pi}{v_F}|\tilde{t}_{l,\alpha}|^2$, the coefficients can be further simplified as $S_{lk}^{\alpha\beta} = -\delta_{l,k}\delta_{\alpha,\beta} + i\sqrt{\tilde{\Gamma}_{l,\alpha}\tilde{\Gamma}_{k,\beta}}/(E - E_M + i\Sigma_{l,\alpha}\tilde{\Gamma}_{l,\alpha})$, where $\tilde{\Gamma}_{l,\alpha} = \frac{\pi}{v_F}|\tilde{t}_{l,\alpha}|^2$ is the effective linewidth function of the α part in the lth lead. The scattering matrices lead to the following relationships:

$$\begin{aligned} T_{\mathrm{CAR}} &= |S_{\mathrm{LR}}^{eh}|^2 \propto |\tilde{t}_{Le}\tilde{t}_{Rh}|^2 \propto 1 - e^{-2L/\xi}\sin(k_F L), \\ T_e &= |S_{\mathrm{LR}}^{ee}|^2 \propto |\tilde{t}_{Le}\tilde{t}_{\mathrm{Re}}|^2 \propto 1 + (-1)^{N_v} 4e^{-L/\xi}\sin(k_F L), \end{aligned}$$

T_{CAR} is proportional to the joint LDOS of both the electron and the hole at the ends of the wire, and T_e is proportional to the electron LDOS at the ends. We can see that the correction of the finite-size effect is a first-order correction to the ET process, and is a second-order correction to the CAR process. The ET process is more sensitive to the phase difference and exhibits a parity-related oscillation behavior. What is more, since the correction factor is in the order of $e^{-L/\xi}$, the length of the wire plays an important role in the interference pattern strength. To observe a clear interference pattern of MQPs, the length of the wire should be one to three times the coherence length.

We have shown that interference in the ET process is a first-order correction while it is a second-order correction in the CAR process. We stress that the insensitivity of the CAR process directly manifests the self-Hermitian property of MQPs. Because of the self-Hermitian property of MQPs, for a hybridized state caused by MQPs, self-Hermitian requires $|u_{\mathrm{end}}|^2 = 1 + b\sin(\phi/2)$ and $|\upsilon_{\mathrm{end}}|^2 = 1 - b\sin(\phi/2)$. No such restrictions hold for usual in-gap states; the electron LDOS is not related to the hole LDOS. In general, $|u_{\mathrm{end}}|^2 = 1 + b\sin(\phi/2)$ and $|\upsilon_{\mathrm{end}}|^2 = 1 - b'\sin(\phi/2)$ can be taken for usual in-gap states. Thus, $T_{\mathrm{CAR}} \propto 1 + (b - b')\sin(\phi/2)$. The first-order interference effect caused by trivial states can be still observed in the CAR process. Indeed, Fig. 2(c) shows that T_{CAR} exhibits some oscillation behavior when the chemical potential lies in the trivial region. Thus, in such a short semiconductor superconducting wire, both the ET and the CAR processes manifest the nonlocal property of MQPs as well as their self-Hermitian property.

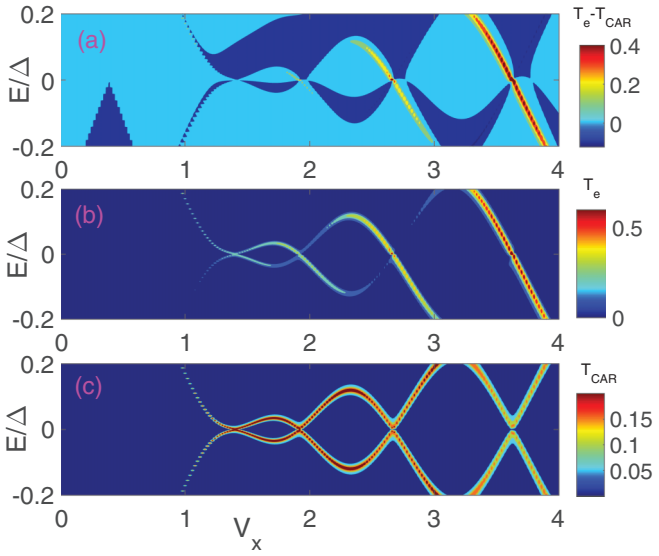

FIG. 3. The Zeeman field can also adjust effective Fermi wave vector well. (a) Contour plot of the total differential conductance from left lead to right lead with incident energy E and Zeeman field V_x. (b) Contour plot of the electron transmission coefficient T_e. (c) Contour plot the crossed Andreev reflection T_{CAR} as a function of incident energy E and Zeeman field V_x. Here the chemical potential lies in $\mu = -95\Delta$, other parameters are the same as before.

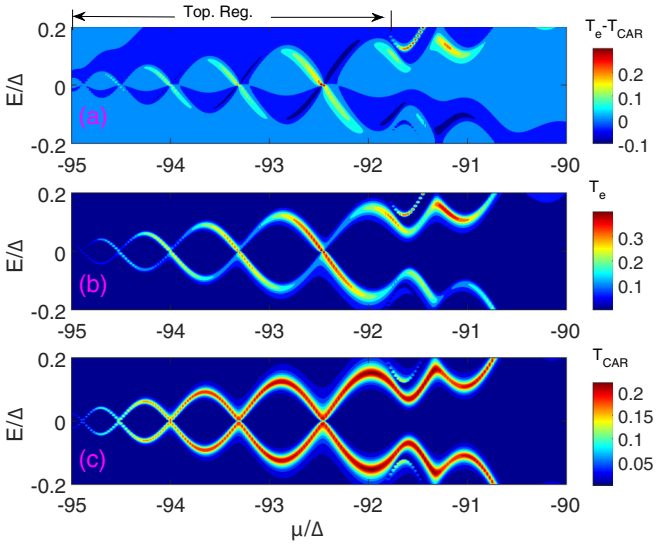

FIG. 4. The disorder effect in our model. The even-odd interference effect is not destroyed by moderate disorder. (a) Contour plot of total differential conductance from left lead to right lead with incident energy E and chemical potential μ. (b) Contour plot of electron transmission coefficient T_e. In this case, the interference effect in the ET process can be well observed. (c) Contour plot of crossed Andreev reflection T_{CAR} as a function of incident energy E and chemical potential μ. Other parameters are $N_x = 100a$, $N_y = 5a$, $U_R = 2\Delta$, $V_x = 2\Delta$, $V_{\mathrm{imp}} = 4\Delta$.

C. Zeeman-field-tuned interference effect

In a semiconductor superconducting wire system, a Zeeman field is an essential tool to induce topological transition. MQPs emerge only in the condition of $V_x > \sqrt{\mu^2 + \Delta^2}$. Thus, studying the effect of a Zeeman field is necessary. In prior sections, we demonstrated that the parity related interference effect can be observed in a short topological superconducting wire through the gate voltage. Herein, we show that the Zeeman field can induce a similar interference effect. Figure 3(a) shows the contour plot of the total tunneling coefficient $T_e - T_{\mathrm{CAR}}$ versus the incident energy E and Zeeman field V_x. As the Zeeman field increases, the system enters into a nontrivial region. After the system enters this topological region, the current exhibits a similar positive-negative exchange behavior with increasing magnetic field. We further divided it into two parts: ET and CAR. Figure 3(b) shows the contour plot of the ET tunneling coefficient T_e as a function of μ and E. The plot clearly shows the interference information. In one region, the interference effect is constructive and T_e is large, while in another region, the interference effect is destructive and T_e is very small. As for the CAR process, Fig. 3(c) shows the contour plot of T_{CAR} versus μ and E, and the interference pattern can hardly be detected here. The Zeeman field can also induce similar even-odd interference effects, just as the chemical potential. The reason is that the Zeeman field can also modulate the effective Fermi wave vector of the system. In prior sections, we showed that $k_F \approx \sqrt{\sqrt{V_x^2 - \Delta^2} + \mu}$. Thus, the Zeeman field can play the same role as the chemical potential; both can modulate the phase by varying the Fermi wave vector. Interestingly, the nonlocal conductance in an NSN junction was studied recently [68]. The authors also displayed the even-odd relation at the topological phase transition point, which are consistent with our results at the transition point as shown in Fig. 3(a).

D. Effect of disorder

We have discussed the interference effect of MQPs and related it to the transport properties in a short wire in the absence of disorder. However, disorder is unavoidable in a real system. In general, MQPs are robust to disorder [69], but the effect of disorder on the interference of two MQPs still requires further study. Interference needs both the state stability and phase coherence. The interference pattern is usually sensitive to disorder and may shifts entirely with small amounts of disorder.

Interestingly, weak disorder does not destroy the even-odd interference effect, on the contrary, it actually seems to enhance it. Figure 4 shows the results in the presence of disorder. We consider the case with on-site disorder that is uniformly distributed over the range $[-V_{\mathrm{imp}}/2, V_{\mathrm{imp}}/2]$ with $V_{\mathrm{imp}} = 4\Delta$. Figure 4(a) shows the contour plot of total differential conductance from the left lead to the right lead with incident energy E and chemical potential μ. The information of the interference effect is clearly observed. Figure 4(b) shows the contour plot of T_e versus the chemical potential and the incident energy while Fig. 4(c) shows the contour plot of T_{CAR} versus the chemical potential and the incident energy. The interference information is also easily observed in the T_e case, but not in the T_{CAR} case. Compared to the results in Fig. (2), the even-odd interference information is even clearer in Fig. 4. We speculate that this is because of the protection of

topology. The MQPs are not destroyed by the weak disorder and neither is the interference information of MQPs. Other transport processes in the topological superconductor system may be easily destroyed by the disorder. Thus, the even-odd interference effect is clearer in the presence of moderate disorder. The numerical results show an enhanced interference region when $V_{\text{imp}} < 6\Delta$.

IV. CONCLUSION

We have shown that the tunneling coefficient of the electron transmission process displays a very interesting even-odd interference behavior. In addition, We have also shown that observing the same behavior in the tunneling coefficient of the CAR process is difficult. The underlying reasons have been further investigated, indicating that the anomalous interference behaviors are directly related to the self-Hermitian property of MQPs. Because of the self-Hermitian property, the interference correction in the electron transmission process is a first-order one, while the correction in the CAR process is a higher-order one. Thus, it is more significant in the ET process than in the CAR process. Such a unique transport property of MQPs demonstrates both the nonlocal and self-Hermitian characteristics of MQPs.

ACKNOWLEDGMENTS

We gratefully acknowledge the support from NSF-China under Grants No. 11574245 (J.L.), No. 11204065 (J.T.S.), No. 11474085 (J.T.S.), No. 11574007 (Q.-F.S.), and No. 11534001 (X.C.X.), National Key R and D Program of China (Grant No. 2017YFA0303301), and NBRP of China (Grant No. 2015CB921102). J.L. was also supported by the China Post-doctoral Science Foundation under Grant No. 2015M580828 and the China Fundamental Research Funds for Central University with Grant No. xjj2015059.

[1] D. A. Ivanov, Phys. Rev. Lett. **86**, 268 (2001).
[2] C. Nayak, S. H. Simon, A. Stern, M. Freedman, and S. Das Sarma, Rev. Mod. Phys. **80**, 1083 (2008).
[3] J. Alicea, Y. Oreg, G. Refael, F. Von Oppen, and M. Fisher, Nat. Phys. **7**, 412 (2011).
[4] A. Kitaev, Phys. Usp. **44**, 131 (2001).
[5] L. Fu and C. L. Kane, Phys. Rev. Lett. **100**, 096407 (2008).
[6] J. D. Sau, R. M. Lutchyn, S. Tewari, and S. Das Sarma, Phys. Rev. Lett. **104**, 040502 (2010).
[7] S. Fujimoto, Phys. Rev. B **77**, 220501(R) (2008).
[8] M. Sato, Y. Takahashi, and S. Fujimoto, Phys. Rev. B **82**, 134521 (2010).
[9] J. Alicea, Phys. Rev. B **81**, 125318 (2010).
[10] R. M. Lutchyn, J. D. Sau, and S. Das Sarma, Phys. Rev. Lett. **105**, 077001 (2010).
[11] Y. Oreg, G. Refael, and F. von Oppen, Phys. Rev. Lett. **105**, 177002 (2010).
[12] A. C. Potter and P. A. Lee, Phys. Rev. B **83**, 094525 (2011).
[13] S. Nadj-Perge, I. K. Drozdov, B. A. Bernevig, and A. Yazdani, Phys. Rev. B **88**, 020407 (2013).
[14] J. Klinovaja, P. Stano, A. Yazdani, and D. Loss, Phys. Rev. Lett. **111**, 186805 (2013).
[15] V. Mourik, K. Zuo, S. M. Frolov, S. R. Plissard, E. P. A. M. Bakkers, and L. P. Kouwenhoven, Science **336**, 1003 (2012).
[16] K. T. Law, P. A. Lee, and T. K. Ng, Phys. Rev. Lett. **103**, 237001 (2009).
[17] M. Wimmer, A. R. Akhmerov, J. P. Dahlhaus, and C. W. J. Beenakker, New J. Phys. **13**, 053016 (2011).
[18] M. T. Deng, C. L. Yu, G. Y. Huang, M. Larsson, P. Caroff, and H. Q. Xu, Nano Lett. **12**, 6414 (2012).
[19] A. Das, Y. Ronen, Y. Most, Y. Oreg, M. Heiblum, and H. Shtrikman, Nat. Phys. **8**, 887 (2012).
[20] H. O. H. Churchill, V. Fatemi, K. Grove-Rasmussen, M. T. Deng, P. Caroff, H. Q. Xu, and C. M. Marcus, Phys. Rev. B **87**, 241401 (2013).
[21] L. P. Rokhinson, X. Liu, and J. K. Furdyna, Nat. Phys. **8**, 795 (2012).
[22] S. Nadj-perge, l. K. Drozdov, J. Li, H. Chen, S. Jeon, J. Seo, A. H. MacDonald, B. A. Bernevig, and A. Yazdani, Science **346**, 602 (2014).
[23] J. Liu, A. C. Potter, K. T. Law, and P. A. Lee, Phys. Rev. Lett. **109**, 267002 (2012).
[24] D. Bagrets and A. Altland, Phys. Rev. Lett. **109**, 227005 (2012).
[25] D. I. Pikulin, J. P. Dahlhaus, M. Wimmer, H. Schomerus, and C. W. J. Beenakker, New J. Phys. **14**, 125011 (2012).
[26] G. Kells, D. Meidan, and P. W. Brouwer, Phys. Rev. B **85**, 060507(R) (2012).
[27] S. Tewari, T. D. Stanescu, J. D. Sau, and S. Das Sarma, Phys. Rev. B **86**, 024504 (2012).
[28] H. Zhang, O. Gul, S. Conesa-Boj, K. Zuo, V. Mourik, F. K. de Vries, J. van Veen, D. J. van Woerkom, M. P. Nowak, M. Wimmer, D. Car, S. Plissard, E. P. A. M. Bakkers, M. Quintero-Prez, S. Goswami, K. Watanabe, T. Taniguchi, and L. P. Kouwenhoven, Nat. Commun. **8**, 16025 (2017).
[29] S. M. Albrecht, A. P. Higginbotham, M. Madsen, F. Kuemmeth, T. S. Jespersen, J. Nygård, P. Krogstrup, and C. M. Marcus, Nature (London) **531**, 206 (2016).
[30] M. T. Deng, S. Vaitiekenas, E. B. Hansen, J. Danon, M. Leijnse, K. Flensberg, J. Nygård, P. Krogstrup, and C. M. Marcus, Science **354**, 1557 (2016).
[31] S. M. Albrecht, E. B. Hansen, A. P. Higginbotham, F. Kuemmeth, T. S. Jespersen, J. Nygård, P. Krogstrup, J. Danon, K. Flensberg, and C. M. Marcus, Phys. Rev. Lett. **118**, 137701 (2017).
[32] B. E. Feldman, M. T. Randeria, J. Li, S. Jeon, Y. Xie, Z. Wang, I. K. Drozdov, B. A. Bernevig, and A. Yazdani, Nat. Phys. **13**, 286 (2017).
[33] S. Hart, H. Ren, T. Wagner, P. Leubner, M. Mülbauer, C. Brüne, H. Buhmann, L. W. Molenkamp, and A. Yacoby, Nat. Phys. **10**, 638 (2014).
[34] V. S. Pribiag, A. J. A. Beukman, F. Qu, M. C. Cassidy, C. Charpentier, W. Wegscheider, and L. P. Kouwenhoven, Nat. Nanotechnol. **10**, 593 (2015).
[35] Y. Pang, J. Shen, J. Wang, J. Feng, F. Qu, Z. Lyu, J. Fan, G. Liu, Z. Ji, X. Jing, C. Yang, Q. Sun, X. C. Xie, L. Fu, and L. Lu, arXiv:1503.00838.
[36] J. Wiedenmann, E. Bocquillon, R. S. Deacon, S. Hartinger, O. Herrmann, T. M. Klapwijk, L. Maier, C. Ames, C. Brune, C. Gould, A. Oiwa, K. Ishibashi, S. Tarucha, H. Buhmann, and L. W. Molenkamp, Nat. Commun. **7**, 10303 (2016).

[37] E. Bocquillon, R. S. Deacon, J. Wiedenmann, P. Leubner, T. M. Klapwijk, C. Brüne, K. Ishibashi, H. Buhmann, and L. W. Molenkamp, Nat. Nanotechnol. **12**, 137 (2016).
[38] R. S. Deacon, J. Wiedenmann, E. Bocquillon, F. Domínguez, T. M. Klapwijk, P. Leubner, C. Brüne, E. M. Hankiewicz, S. Tarucha, K. Ishibashi, H. Buhmann, and L. W. Molenkamp, Phys. Rev. X **7**, 021011 (2017).
[39] D. J. van Woerkom, A. Proutski, B. van Heck, D. Bouman, J. I. Väyrynen, L. I. Glazman, P. Krogstrup, J. Nygård, L. P. Kouwenhoven, and A. Geresdi, Nat. Phys. **13**, 876 (2017).
[40] K. Zuo, V. Mourik, D. B. Szombati, B. Nijholt, D. J. van Woerkom, A. Geresdi, J. Chen, V. P. Ostroukh, A. R. Akhmerov, S. R. Plissard, D. Car, E. P. A. M. Bakkers, D. I. Pikulin, L. P. Kouwenhoven, and S. M. Frolov, Phys. Rev. Lett. **119**, 187704 (2017).
[41] M. F. Goffman, C. Urbina, H. Pothier, J. Nygård, C. M. Marcus, and P. Krogstrup, New J. Phys. **19**, 092002 (2017).
[42] L. Fu and C. L. Kane, Phys. Rev. B **79**, 161408 (2009).
[43] J. Cayao, arXiv:1703.07630 (2017).
[44] J. Cayao, E. Prada, P. San-Jose, and R. Aguado, Phys. Rev. B **91**, 024514 (2015).
[45] P. San-Jose, J. Cayao, E. Prada, and R. Aguado, New J. Phys. **15**, 075019 (2013).
[46] P. San-Jose, E. Prada, and R. Aguado, Phys. Rev. Lett. **108**, 257001 (2012).
[47] F. Domínguez, F. Hassler, and G. Platero, Phys. Rev. B **86**, 140503(R) (2012).
[48] F. Crepin and B. Trauzettel, Phys. Rev. Lett. **112**, 077002 (2014).
[49] M. Houzet, J. S. Meyer, D. M. Badiane, and L. I. Glazman, Phys. Rev. Lett. **111**, 046401 (2013).
[50] J. J. He, T. K. Ng, P. A. Lee, and K. T. Law, Phys. Rev. Lett. **112**, 037001 (2014).
[51] H.-H. Sun, K.-W. Zhang, L.-H. Hu, C. Li, G.-Y. Wang, H.-Y. Ma, Z.-A. Xu, C.-L. Gao, D.-D. Guan, Y.-Y. Li, C. Liu, D. Qian, Y. Zhou, L. Fu, S.-C. Li, F.-C. Zhang, and J.-F. Jia, Phys. Rev. Lett. **116**, 257003 (2016).
[52] J. Liu, F.-C. Zhang, and K. T. Law, Phys. Rev. B **88**, 064509 (2013).
[53] J. Nilsson, A. R. Akhmerov, and C. W. J. Beenakker, Phys. Rev. Lett. **101**, 120403 (2008).
[54] P. Wang, J. Liu, Q.-f. Sun, and X. C. Xie, Phys. Rev. B **91**, 224512 (2015).
[55] Y.-T. Zhang, Z. Hou, X. C. Xie, and Q.-F. Sun, Phys. Rev. B **95**, 245433 (2017).
[56] L. Fu, Phys. Rev. Lett. **104**, 056402 (2010).
[57] S. S. Hegde and S. Vishveshwara, Phys. Rev. B **94**, 115166 (2016).
[58] G. Ben-Shach, A. Haim, I. Appelbaum, Y. Oreg, A. Yacoby, and B. I. Halperin, Phys. Rev. B **91**, 045403 (2015).
[59] S. Vijay and L. Fu, Phys. Rev. B **94**, 235446 (2016).
[60] T. Karzig, C. Knapp, R. M. Lutchyn, P. Bonderson, M. B. Hastings, C. Nayak, J. Alicea, K. Flensberg, S. Plugge, Y. Oreg, C. M. Marcus, and M. H. Freedman, Phys. Rev. B **95**, 235305 (2017).
[61] A. M. Lobos, and S. Das Sarma, New J. Phys. **17**, 065010 (2015).
[62] A. Zazunov, R. Egger, and A. L. Yeyati, Phys. Rev. B **94**, 014502 (2016).
[63] E. Prada, P. San-Jose, and R. Aguado, Phys. Rev. B **86**, 180503(R) (2012).
[64] S. Das Sarma, J. D. Sau, and T. D. Stanescu, Phys. Rev. B **88**, 220506(R) (2013).
[65] D. Rainis, L. Trifunovic, J. Klinovaja, and D. Loss, Phys. Rev. B **87**, 024515 (2013).
[66] J. J. He, J. Wu, T.-P. Choy, X.-J. Liu, Y. Tanaka, and K. T. Law, Nat. Commun. **5**, 3232 (2014).
[67] A. Yamakage and M. Sato, Physica E **55**, 13 (2014).
[68] T. Ö. Rosdahl, A. Vuik, M. Kjaergaard, and A. R. Akhmerov, arXiv:1706.08888.
[69] O. A. Awoga, K. Björnson, and A. M. Black-Schaffer, Phys. Rev. B **95**, 184511 (2017).